Radio meteors above the Arctic Circle: radiants, orbits and estimated magnitudes

Csilla Szasz

RADIO METEORS ABOVE THE ARCTIC CIRCLE:
RADIANTS, ORBITS AND ESTIMATED MAGNITUDES

Akademisk avhandling

som med vederbörligt tillstånd av rektorsämbetet vid Umeå universitet
för avläggande av teknologie doktorsexamen i rymdteknik framlägges
till offentlig granskning i IRF:s aula, tisdagen den 6 maj 2008, kl. 9:00

av

Csilla Szasz

FAKULTETSOPPONENT
Dr. Noah Brosch, Tel Aviv University, Tel Aviv, Israel

IRF

RADIO METEORS ABOVE THE ARCTIC CIRCLE:
RADIANTS, ORBITS AND ESTIMATED MAGNITUDES

Csilla Szasz

RADIOMETEORER OVAN POLCIRKELN:
RADIANTER, BANOR OCH UPPSKATTADE MAGNITUDER

Cover illustration:

The sun, the Earth and 39 meteoroid orbits

BLUE CURVES: Orbits of Earth (⊕), Mars (♂), Jupiter (♃) and Saturn (♄) around the sun (☉)
GREEN CURVES: prograde meteoroid orbits
RED CURVES: retrograde meteoroid orbits

CSILLA SZASZ and JOHAN KERO

Radiometeorer ovan polcirkeln:
radianter, banor och uppskattade magnituder

Sammanfattning

Avhandlingens resultat är baserade på mätningar med den trestatiska EISCAT UHF-radarn och tre SKiYMet meteorradarsystem. En metod för meteoroidbanberäkning presenteras i detalj.

EISCAT UHF-systemet består av tre identiska, 32 m stora parabolantenner: en hög-effektssändare/mottagare och två fjärrstyrda mottagare. Under fyra 24-timmarsmätningar vid vår-/höstdagjämning och sommar-/vintersolstånd mellan 2002 och 2005 detekterades 410 meteoriska huvudekon simultant med alla tre mottagare. Dessa trestatiska meteorers atmosfärsinbromsning och radartvärsnitt har fastställts mycket noggrant och använts till att beräkna meteoroidernas banor samt uppskatta meteorernas luminositeter. Ingen av de observerade meteoroiderna verkar vara av interstellärt eller asteroidursprung. Deras troligaste ursprung är kometer, framför allt kortperiodskometer ($<$ 200 år). Ungefär 40% av meteorradianterna kan associeras till norra apex, ett källområde för sporadiska meteorer, och totalt är 58% av partiklarnas banor retrograda. Meteoroidernas geocentriska hastighetsfördelning har två lokala maxima: ett för den prograda populationen vid 38 km/s och ett för den retrograda vid 59 km/s. Genom att anpassa datat till en numerisk ablationsmodell som simulerar meteoroidernas färd genom atmosfären har de detekterade meteorernas absoluta visuella magnituder uppskattats till mellan +9 och +5. Detta innebär att de är observerbara med bildförstärkta, teleskopiska CCD-kameror.

Avhandlingen diskuterar även hur sporadiska meteorers dygns- och säsongsinflöde beror på geografisk latitud och meteorradianternas distribution på himmelssfären. Detta utreds med hjälp av spårekon detekterade under perioden 1999-2004 med tre meteorradarsystem på latituderna 68°N, 55°N och 8°S. Dygnsinflödet varierar mest på låga latituder och minst på höga. Ju högre latitud, desto mer förändras däremot dygnsinflödet över året. Avhandlingen visar att de dominerande källområdena varierar med säsong, över dygnet och med latitud.

Både EISCAT UHF-systemet och meteorradarn på 68°N är belägna nära polcirkeln. Detta innebär att norra ekliptiska polen (NEP) är i zenit en gång per dygn, året om. Vid just denna tidpunkt sammanfaller ekliptikan med den lokala horisonten, vilket möjliggör att det observerade meteorinflödet från norra ekliptiska hemisfären kan jämföras över året. Under timmen då NEP är närmast zenit har EISCAT UHF uppmätt ett ungefär tre gånger högre meteorinflöde vid sommarsolståndet än under de andra säsongerna, vilket överensstämmer med resultaten från meteorradarn på 68°N.

RADIO METEORS ABOVE THE ARCTIC CIRCLE:
RADIANTS, ORBITS AND ESTIMATED MAGNITUDES

ABSTRACT

This thesis presents results based on data collected with the 930 MHz EISCAT UHF radar system and three SKiYMet specular meteor radars. It describes in detail a method for meteoroid orbit calculation.

The EISCAT UHF system comprises three identical 32 m parabolic antennae: one high-power transmitter/receiver and two remote receivers. Precise meteoroid deceleration and radar cross section are determined from 410 meteor head echoes simultaneously observed with all three receivers between 2002 and 2005, during four 24 h runs at the summer/winter solstice and the vernal/autumnal equinox. The observations are used to calculate meteoroid orbits and estimate meteor visual magnitudes. None of the observed meteors appear to be of extrasolar or asteroidal origin; comets, particularly short period (< 200 years) ones, may be the dominant source for the particles observed. About 40% of the radiants are associated with the north apex sporadic meteor source and 58% of the orbits are retrograde. The geocentric velocity distribution is bimodal with a prograde population centred around 38 km/s and a retrograde population peaking at 59 km/s. The absolute visual magnitudes of meteors are estimated to be in the range of +9 to +5 using a single-object numerical ablation model. They are thus observable using intensified CCD cameras with telephoto lenses.

The thesis also investigates diurnal meteor rate differences and sporadic meteor radiant distributions at different latitudes using specular meteor trail radar measurements from 68°N, from 55°N and from 8°S. The largest difference in amplitude of the diurnal flux variation is at equatorial latitudes, the lowest variation is found at high latitudes. The largest seasonal variation of the diurnal flux is observed with the high-latitude meteor radar. The investigations show a variation in the sources with both latitude and time of day.

The EISCAT UHF system and the high-latitude meteor radar are located close to the Arctic Circle. Such a geographical position means that zenith points towards the North Ecliptic Pole (NEP) once every day all year round. This particular geometry allows the meteoroid influx from the north ecliptic hemisphere to be compared throughout the year as the ecliptic plane coincides with the local horizon. Considering only the hour when NEP is closest to zenith, the EISCAT UHF head echo rate is about a factor of three higher at summer solstice than during the other seasons, a finding which is consistent with the high-latitude meteor radar measurements.

CONTENTS

LIST OF INCLUDED PAPERS

This thesis is based on the work reported in the following papers:

I. C. Szasz, J. Kero, D. D. Meisel, A. Pellinen-Wannberg, G. Wannberg, and A. West-man (2008). ORBIT CHARACTERISTICS OF THE TRISTATIC EISCAT UHF METEORS, Monthly Notices of the Royal Astronomical Society, submitted.

II. C. Szasz, J. Kero, A. Pellinen-Wannberg, D. D. Meisel, G. Wannberg, and A. West-man (2008). ESTIMATED VISUAL MAGNITUDES OF THE EISCAT UHF METEORS, Earth, Moon, and Planets, 102:373–378.

III. C. Szasz, J. Kero, A. Pellinen-Wannberg, J. D. Mathews, N. J. Mitchell, and W. Singer (2004). LATITUDINAL VARIATIONS OF DIURNAL METEOR RATES, Earth, Moon, and Planets, 95:101–107.

IV. C. Szasz, J. Kero, A. Pellinen-Wannberg, G. Wannberg, A. Westman, N. J. Mitchell, and W. Singer (2005). RADAR STUDIES OF THE SPORADIC METEOROID COMPLEX, In Proceedings of RadioVetenskap och Kommunikation, Linköping, 2005, pp. 191–196, FOI and Tekniska högskolan Linköpings universitet, June 14-16.

V. D. D. Meisel, C. Szasz, and J. Kero (2008). QUANTITATIVE COMPARISON OF A NEW AB INITIO MICROMETEOR ABLATION MODEL WITH STANDARD PUBLISHED MODELS, Earth, Moon, and Planets, 102:411–415.

The papers have been reprinted with permission from the publishers, and are included as appendices to this thesis.

1 INTRODUCTION TO METEOR PHYSICS

METEOROIDS roam through the solar system with orbits of all inclinations. Meteoroids, or interplanetary/interstellar debris, range in size from small asteroids with radii of ~10 km down to micrometeoroids with radii of ~100 µm and dust, radii ~1 µm (Beech and Steel, 1995). Meteor, colloquially "shooting star", is the common name for the streak of light in the sky generated by meteoroids and other natural bodies entering the terrestrial atmosphere irrespective of size, structure and origin (Beech and Steel, 1995). If any material survives the plunge through air, it strikes the ground as a meteorite.

The word meteor originates from the Greek word $\mu\varepsilon\tau\varepsilon\omega\rho o\nu$ meaning an atmospheric phenomenon, as rain, hail, snowfall, lightning, thunder, storm, rainbow and shooting star (Meteor, 1944). Today the word meteorology is used to denote weather processes and meteor means only shooting star.

Meteoroids bound up in the solar system colliding with the Earth's atmosphere have geocentric speeds ranging from the Earth escape velocity of 11.2 km/s to the solar escape velocity of 72.3 km/s (Ceplecha et al., 1998). Interplanetary meteoroids cannot have speeds exceeding the solar escape velocity at the Earth orbit, i.e. 42.5 km/s in the solar frame of reference, and Earth moves along its orbit at a speed of 29.8 km/s. Meteoroids with greater speeds than 42.5 km/s have hyperbolic orbits and thus originate from interstellar space (Zeilik and Gregory, 1998).

Sporadic meteors can be seen every night with the naked eye in all possible directions. About 75% of the observed meteors are sporadic, the rest belong to meteor showers (Ceplecha et al., 1998). Meteor showers occur when Earth cuts through comet trails. Comets can simply be described as dusty balls of snow and ice. Therefore, as a result of intense solar heating and tidal forces, comets leave material lost from their tail behind in the form of pieces of solid material as they approach the sun (Zeilik and Gregory, 1998). When Earth intercepts the orbit of a comet, meteors seem to come from a certain point in the sky, called the meteor radiant, when their trails are traced back on a sky map. Meteor showers are usually named after the constellations in which their radiants lie. Examples of spectacular yearly showers are the Perseid shower appearing in August, the Leonid shower in November and the Geminid shower in December.

When a meteoroid enters the atmosphere, it may be heated to several thousand Kelvin by friction due to air molecules. Meteoroids of sizes between 0.05 and 0.5 mm are heated throughout while only the surface layer, down to a few tenths of a millimeter, is heated for larger particles (Ceplecha et al., 1998). Depending on size and velocity, it takes about 10 to 40 km before a meteoroid has lost all of its mass (Ceplecha et al., 1998). The time duration for visible meteors is on average less than one second.

After atmospheric entry the meteoroid starts to heat up. Before the melting point is reached, the heat input is balanced by a temperature rise in the body and thermal radiation from it. However, the temperature cannot rise higher than the boiling point of the meteoroid and mass is therefore lost through ablation – meteoroid mass loss due to vaporization, fusion of molten material and fragmentation (Bronshten, 1983). The visible light emitted from the meteoroid arises mostly from the deexcitation of the excited atoms lost from the the surface of the meteoroid (Ceplecha et al., 1998; Hawkes, 2002). The process ends with the meteoroid either disappearing via ablation or dropping below the boiling temperature and impacting the ground – as a meteorite. Slow

meteoroids smaller than a few hundreds of micrometres do not reach the evaporation regime at all, thus no meteor phenomena occur. Instead, a meteoroid dust particle sediments slowly through the atmosphere and reaches the Earth surface unchanged (Ceplecha et al., 1998), but they can also be melted, or partially melted (Genge, 2008). The main ablation occurs within the height range from 140 to 70 km (Hawkes, 2002), where the atmospheric pressure starts to be significant. The density of the atmosphere increases and the size of the meteoroid decreases due to ablation during the downward flight.

A meteoroid also decelerates during its atmospheric passage, but by no more than a few percent (Ceplecha et al., 1998; Hawkes, 2002; Herlofson, 1951). Millimeter-sized meteoroids or smaller are in free molecular flow during flight in the atmosphere (Bronshten, 1983). Thus collisions with single air molecules are the most important process during their passage through the atmosphere. Considering a typical meteoroid with a velocity of about 40 km/s, most collisions between air molecules and the meteoroid surface will be inelastic and the excess velocity will heat the body. Furthermore, the binding energy of the meteoroid atoms is as low as a few electron volts, thus the energy of one trapped air molecule is sufficient to evaporate a large number of meteoroid atoms. This means that intercepting an air mass of 1-2 % of the meteoroid mass is enough to entirely disrupt the meteoroid into atoms (Herlofson, 1951). In particular, it is observationally confirmed that since the intercepted air mass is negligible compared to the meteoroid mass, the body will generally not be decelerated more than a few percent before it is disrupted into separate atoms.

The jet of vaporised atoms emerging from the meteoroid, mixed with air, is called coma in the area where the atoms are not fully decelerated yet, i.e. where these elements still have a considerable portion of their original kinetic energy of forward motion left. The main dissipation of the ordinary meteoroids take place in the coma and it is also here the impact radiation takes place, which means that the coma is the main source of the luminosity of visible meteors. At an adequate distance behind the coma is the wake train, a region where the translational velocity of the coma is decelerated well below the mean molecular velocity of the surrounding atmosphere. The wake train has the shape of a column that is tailing the meteoroid, also called the trail and is the same ionized column observed with specular radars (see Section 3.1). Bright and fast meteors are after their disappearance followed by a band of light called the train. The diameter of the train is in the order of 0.1 to 1 km and its time of visibility ranges from a few seconds to several minutes. A more detailed description of the meteor phenomenon can be found in Öpik (1958).

2 Sources of Meteoroids

LTHOUGH the lifetime of dust particles in the solar system is of the order of only 10^5 years, hypervelocity microimpact craters on larger grains of meteoritic and lunar origin attests that dust has existed in interplanetary space for billions of years (Brownlee, 1985). This implies that new dust is created continuously.

Dust grains in interplanetary space have finite lifetimes. They will eventually escape the solar system on hyperbolic paths or fall into the Sun. The escape scenario takes place if the solar radiation pressure force on a particle is stronger than the gravitational force (Williams, 2002). Particles on bound orbits will decelerate due to the Poynting-Robertson effect, which make their orbits shrink more and more until they are finally destroyed by the heat of the Sun. The inner parts of this dust population is seen as the zodiacal light.

All solid bodies in the solar system can release material during impact events. As impact events large enough for releasing particulates from planets have been rare, at least during the second half of the solar system lifetime, comets and asteroids are the main sources of dust (Brownlee, 1985). Active comets produce dust and meteoroids during ice sublimation as they approach perihelion. Asteroids can only generate dust through collisions.

2.1 Discriminating Cometary Dust from Asteroidal Dust

Comets are icy protoplanets formed during the nebular evolution in the outskirts of the solar system. This region is called the Oort cloud and defines a spherical region with a radius of 10^5 AU. Long-period comets have their aphelia in the Oort cloud whereas most short-period comets reside in the Kuiper belt, a region at a distance of about 40-50 AU from the Sun. The primordial dust incorporated in an icy protoplanet will be released to interplanetary space if the orbit of the body gets perturbed and it reaches the inner parts of the solar system. As the body approaches perihelion, it will eject dust in a tail-like manner characteristic for an active comet. The dust grains will have velocities of the same order as their parent body.

The velocity of cometary dust will at 1 AU be significantly higher than the velocity of dust released by collisions of asteroids in the asteroid belt. The most obvious way of discriminating between dust from comets and asteroids is therefore velocity and orbit determination (Jessberger, 2001).

Cometary dust is more primitive than asteroidal dust in the sense that it has not been altered by the thermal and aqueous processes taking place inside asteroids (Rietmeijer, 2002). The dynamic pyrometamorphism during atmospheric entry is by far the most dramatic thermal event experienced by collected dust particles.

3   Radar Observations of Meteors

HERE ARE several methods of observing meteors and each method answers different questions. The oldest observations were made with the naked eye. Visual observations in the form of photography, LLLTV (low light level television) and video methods are still widely used, but meteors can also be observed using spectral, lidar, acoustic, infrasonic, seismic and radar methods. Ceplecha et al. (1998) have written an excellent review covering all these observation techniques. Beyond this point, only radar observations will be considered, except in Paper II where simultaneous meteor observations using telescopic optical devices and the EISCAT 930 MHz UHF radar system are discussed.

The radar target is provided by the coherent reflection from the meteor plasma and there are two types of meteor echoes – meteor head echoes and meteor trail echoes. Head echoes are radio wave reflections from the plasma generated by the interaction of meteoroids with the atmosphere at about 70-140 km altitude. The echoes are characterized by being transient and Doppler-shifted. The received power is confined in range, as from a point source, and it moves with the line-of-sight velocity of the meteoroid. Trail echoes are radio wave reflections from the meteor wake train.

3.1   Specular Meteor Radars

The free electrons in the meteor wake train are able to scatter incident radio waves and hence the meteor can be detected by radar systems.

Meteor radar systems operate typically in the 15 to 60 MHz frequency range. Too low frequencies result in interference from ionospherically reflected signals. If the frequency is higher than the ceiling limit, the wake train radius is of the same order as half the wavelength. The wake train then becomes invisible for the radar due to destructive interference between signals reflected at different depths within the wake train (Mitchell, 2002).

A specular meteor radar consists usually of Yagi antennae in various configurations. So-called all-sky systems use low-gain antennae as these are capable of detecting meteors over the whole sky. An example of an all-sky system is the All-Sky Interferometric Meteor Radar called SKiYMet, described in detail by Hocking et al. (2001). One such radar is located at Esrange in northern Sweden. It uses an array consisting of five receiver antennae acting as an interferometer. The five receiving antennae are arranged in the form of an asymmetric cross, with arms of lengths of either 2 or 2.5 wavelengths, as shown in Figure 1. Each receiver antenna is connected to a separate receiver with cables of equal phase-length, about 70 m.

The beam width is defined by the antenna geometry together with the radar frequency. For specular meteor radars, the beam width is tens of degrees and can even approach a cone of π sr (a quarter of a sphere), which is useful if the intention is to study sporadic meteors. Since specular meteor radars have large opening angles, they detect scatter from meteors in a large volume at meteoric heights. In this way, it is possible to observe both shower and sporadic meteors with these radars.

If the plasma trail produced by a meteoroid entering the atmosphere is aligned
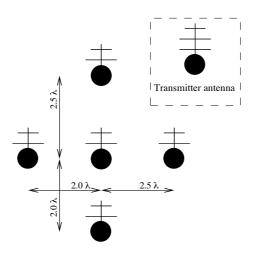
Figure 1: Plan view of the antenna arrangement for the SKiYMet radar system. The placing of the transmitter antenna is arbitrary as long as it is not too close to any of the receiving antennae.

perpendicularly to the meteor radar beam direction, detection may occur. After reflection from ionization trails of incident meteoroids, the echo is received by the receiver antenna array. The interferometric capabilities of the radars enable determination of meteor radiants common to many meteors statistically as described by, e.g., Morton and Jones (1982), Hocking et al. (2001) and in Paper IV. It is not possible to deduce radiants for individual meteors, however, unless the meteor radar system consists of several receiver arrays. Examples are the Advanced Meteor Orbit Radar (AMOR) (Baggaley et al., 1994) and the Canadian Meteor Orbit Radar (CMOR) (Webster et al., 2004; Jones et al., 2005). These systems have run practically continuously since 1990 (AMOR) and 2001 (CMOR) and have recorded millions of meteoroid orbits (Galligan and Baggaley, 2004; Campbell-Brown, 2007). Paper I contains a comparison of the orbits determined by the EISCAT UHF system and results from these and other radar systems.

3.2   HPLA RADARS

The first meteor investigations with what today is termed a High Power Large Aperture (HPLA) radar were conducted by Evans (1965, 1966) with the 440 MHz Millstone Hill radar. Some of the measurements were optimized to provide specular trail reflections (Evans, 1965) whereas others were optimized for detecting head echoes of shower meteoroids travelling down-the-beam (Evans, 1966). Evans pointed the radar beam at shower radiants when these were visible at very low elevations to get as big a cross-beam detection volume as possible and applied strict restrictions to ensure that the detections originated from meteoroids confined in a small angle from boresight.

Dedicated meteor observations were hereafter not conducted with HPLA radars for about 30 years. When studies of meteors with this kind of radar resumed, the improved signal processing techniques and large data handling capacities proved them suitable for studies of sporadic meteor head echoes (Pellinen-Wannberg and Wannberg, 1994; Zhou et al., 1995). The sporadic meteoroids will in general neither travel down the beam nor perpendicular to it and cannot be treated as such (Kero et al., 2008a).

HPLA radars have very narrow beams; the opening angle is usually less than $1°$. Therefore, when using a narrow-beam radar, a head echo does not usually depict the whole meteor ionization process to which the meteoroid gives rise on its way down through the atmosphere. If the meteoroid does not go straight down the beam, but at some angle to it, only a part of the ionization process is detectable.

4 OBSERVATIONS

HE RESULTS in the appended papers are based on both EISCAT UHF head echo observations and data from three SKiYMet specular meteor trail radars located at equatorial-, mid- and high latitudes. The high-latitude one, the Esrange specular meteor radar, is located only 120 km south-west of the ground projection of the EISCAT tristatic measurement volume, making the meteor influx measurements with the two systems comparable (Paper I).

4.1 EISCAT UHF OBSERVATIONS

The tristatic EISCAT 930 MHz UHF radar system consists of three 32 m paraboloids. The transmitter/receiver is located outside Tromsø, Norway, at 69.59°N, 19.23°E. The two remote receivers are sited in Kiruna, Sweden, at 67.86°N, 20.44°E and Sodankylä, Finland, at 67.36°N, 26.63°E. All three antennae were pointed towards a common volume centered at a height of 96 km, the peak of the meteor altitude distribution of previous EISCAT UHF measurements (Westman et al., 2004). The coordinates of the common volume is 68.88°N, 21.88°E and the configuration used is of tetrahedron geometry as schematised in Figure 2. The –3 dB beamwidths of the antennae are about 0.7°.

For meteor head echoes detected by all three receivers simultaneously, the precise geocentric meteoroid velocity can be calculated. The velocity components measured by the remote receivers point in the directions of the bisectors, defined in the plane spanned by each remote receiver's line-of-sight and the transmitter's line-of-sight. By using the velocity components along the bisectors and the Tromsø line-of-sight as described in detail by Kero et al. (2008a) we estimate the directions of arrival as accurately as possible.
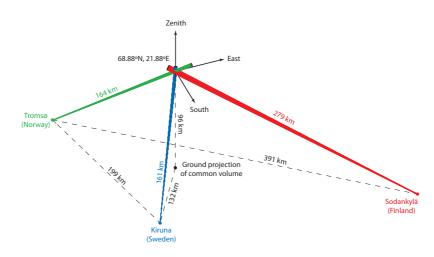

Figure 2: Meteor observing geometry of the EISCAT UHF system. Ranges from the transmitter/receiver and the two remote receivers to the common volume are indicated as well as ground distances between the sites. The full beam widths are plotted as 1° and are drawn to scale.

Table 1: Dates and times for meteor campaigns with the EISCAT UHF system.

	Year	Start – Stop (UT)	No of events
Vernal equinox	2002	Mar 19–20, 12:00–12:00	50
Summer solstice	2005	Jun 21–22, 14:00–10:00	} 101
	2005	Jun 23, 10:00–14:00	
Autumnal equinox	2005	Sep 21–22, 07:00–07:00	194
Winter solstice	2004	Dec 21–22, 08:00–08:00	65

Furthermore, we calculate the speed along the meteoroid trajectory as a function of time for each meteoroid by assuming that it moves along a straight line through the measurement volume. In reality, owing to the Earth's gravity, a meteoroid will follow acurved path but the deviation from linearity during the few kilometres of its trajectory within the common volume is small compared to measurement uncertainties.

The results presented in Papers I and II are based on data collected with the EISCAT UHF system in four dedicated meteor experiments. A total number of 96 h of data were taken between 2002 and 2005, resulting in detection of 410 tristatic meteors. The dates and times for the observations are summarized in Table 1. The seasons apply to the northern hemisphere.

Results from the EISCAT UHF winter solstice measurements also appear in Paper IV. There is a contradiction between the number of tristatic meteors detected during this campaign as given in Table 1 and as stated in Paper IV. The discrepancy is due to a search routine developed to force echoes with strong SNR (signal-to-noise ratio) detected with one or two receiver/-s out of the data of the other/-s. This is possible because the automatic search routine initially finds the events with high SNR but does not necessarily find the ones with (very) low SNR. In other words, several events have low SNR and provide only a few data points from one or two of the receivers but good SNR and a long series of measurements from the other/-s. A few data points from each receiver are enough for an accurate direction determination. If at least one of the receivers provides a long sequence of data the meteoroid deceleration can also be deduced. A more detailed description of the measurement technique and data handling is given by Kero et al. (2008a). In this way, an additional 18 tristatic meteors have been found in the winter solstice data since the publication of Paper IV and are included in later results (Papers I and II).

Our tristatic data give us precise particle deceleration and radar cross sections (Kero et al., 2008a,b), which we have compared and fitted to a single-object ablation model with atmospheric data provided from the MSIS-E-90 atmosphere model (Hedin, 1991). The ablation model implementation is further described in Paper II and in detail by Kero (2008) and allows us to estimate the meteoroid atmospheric entry velocities, needed to calculate the meteoroid orbits as described in Section 6.

The most important feature of the ablation model is that we have used four different meteoroid densities, 0.3 g/cc for porous, 1 g/cc for cometary, 3.3 g/cc for asteroidal and 7.8 g/cc for iron material, paired with mean molecular mass of ablated vapour of 20 u for graphite (both porous and cometary material), 50 u for silicon dioxide and 56 u for iron respectively (Tielens et al., 1994; Rogers et al., 2005). For every meteoroid individually, each pair of density and molecular mass was propagated down through the atmosphere using every one of five different heat transfer coefficients, 0.2, 0.4, 0.6, 0.8 and 1 for each step through the atmosphere. Each combination was fitted to the data by iteratively adjusting the input parameters (above-atmosphere velocity, mass, density and zenith angle) and minimizing the least-square difference between model and measurements. Then the best of the fits was chosen and its input values used as esti-

mates for the extra-atmospheric properties of our observed meteoroids. Thus we obtain extra-atmospheric properties of our observed meteoroids and can determine their orbits (see Section 6, and Paper I), magnitudes (Paper II), etc. The mass distribution found by this method is similar to the one reported for the Advanced Research Projects Agency Long-Range Tracking and Instrumentation Radar (ALTAIR) by Close et al. (2007).

4.2   SKiYMet Specular Radar Observations

In Papers III and IV, specular meteor radar data was used from three different latitudes: Esrange, Kiruna, Sweden, at 67.88°N, 21.12°E; Juliusruh, Germany, at 54.63°N, 13.40°E; and Ascension Island, at 7.95°S, 14.38°W.

Five days of data around each vernal/autumnal equinox and summer/winter solstice was chosen from all data available for all three specular radars. Data periods range from August 1999 to March 2004 for Esrange, from November 1999 to August 2001 for Juliusruh and from May 2001 to November 2003 for Ascension Island.

The data used was recorded by a SKiYMet all-sky interferometric meteor radar at each site (see Section 3.1). Electromagnetic pulses are radiated by the transmitter at a pulse repetition frequency of 2144 Hz. The Esrange and Ascension Island meteor radars operate at 32.50 MHz in the 70-110 km height range. The corresponding figures for the Juliusruh radar are 32.55 MHz and 78-120 km. This radar was transferred to Andøya, Norway, in September 2001 (Singer et al., 2004).

5 COORDINATE SYSTEMS

PHERICAL COORDINATE SYSTEMS are, for obvious reasons, the most useful ones for mapping the sky. Indeed, mapping the sky is important when calculating meteoroid orbits from radar measurements. This section contains a summary of the coordinate systems used for orbit calculations as will be described in Section 6. Spherical coordinates can be thought of as positions on a spherical surface. A plane passing through the center of the sphere – intersecting it in a great circle – perpendicularly to the axis of rotation is called the primary circle. Any great circle perpendicular to the primary circle is called a secondary circle.

5.1 THE LONGITUDE-LATITUDE SYSTEM ON EARTH

One well-known example of a spherical coordinate system is the longitude-latitude system on Earth, where the equator is the primary circle. The meridians are secondary circles, each of which pass through both poles. Positions are given in longitude and latitude. Longitude is the shortest angular distance either in the east or west direction from the prime meridian (through Greenwich, England) along the equator to the point where the meridian through the point of interest crosses the equator. Latitude is the shortest angular distance along this meridian from the equator in the north or south direction to the point of interest.

The Earth is not a perfect sphere. Moreover, the Earth surface has gravitational irregularities due to density and shape variations in the Earth's crust (Roy, 1988). The geocentric latitude assumes a spherical Earth, the astronomical latitude is the geocentric latitude corrected for the flattening of the Earth, and the geodetic or geographic latitude is the astronomical latitude corrected for gravity fluctuations. Geodetic latitude is the one in most common daily use. More detailed descriptions are given by, e.g., Zeilik and Gregory (1998), Danby (1988) and Roy (1988).

The longitude-latitude system is, however, not sufficient to describe celestial phenomena. Instead, there are a number of other spherical coordinate systems which are more suited for that purpose. A common tool for many of the coordinate systems described below is the celestial sphere. It is a stationary sphere with a far greater radius than that of the Earth, surrounding and co-centered with the Earth (Roy, 1988). On the inside of the celestial sphere, all kinds of heavenly bodies are projected.

5.2 THE HORIZON SYSTEM

The horizon, or horizontal, system of coordinates is used for local observations and is therefore different for observers located at different sites on the Earth's surface. A coordinate system with the observer as origin of coordinates is called topocentric (Wilkins and Springett, 1977). This implies that the coordinates for one particular object at one particular time is location-dependent. Also, the horizon system co-rotates with the
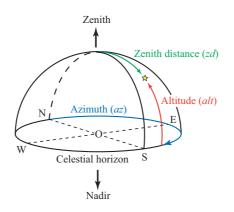
Figure 3: Sketch of the horizon system. N, E, S and W represent the four cardinal points North, East, South and West respectively.

Earth and thus the coordinates for one and the same object changes with time.

The origin of the horizon system is the observer, marked with O in Figure 3. The point where the upward vertical from the observer intersects the celestial sphere is called zenith, the opposite of which is nadir. Let these two points span an axis. A plane perpendicular to this axis intersects the celestial sphere at the celestial horizon and divides the sphere into two hemispheres. To the observer, only the upper hemisphere is visible, even if the actual horizon is for topographic reasons very seldom equal to the celestial one.

The coordinates used to specify an observed object in the horizon system are the azimuth (az) and altitude (alt), or alternatively the azimuth and the zenith distance (zd). One of several definitions of azimuth, and the one used throughout this thesis, is the angular distance along the celestial horizon from the north point (marked with N in Figure 3) eastwards to the point where a vertical circle through zenith and the observed phenomenon intersects the celestial horizon. The azimuth can range from $0°$ to $360°$. The altitude is then the shortest angular distance along this vertical circle measured from the celestial horizon to the object. Zenith is located at $90°$ altitude. The zenith distance is the opposite of the altitude, i.e., it is measured from zenith towards the celestial horizon along the same vertical circle. Hence,

$$zd = 90° - alt. \tag{1}$$

This description of the horizon system is adapted from Zeilik and Gregory (1998), Roy (1988) and Green (1988).

5.3   THE CELESTIAL EQUATORIAL SYSTEM

The most important astronomical coordinate system is the celestial equatorial system, which is illustrated in Figure 4. The two coordinates are right ascension (α) and declination (δ), which closely correspond to the terrestrial longitude and latitude, respectively. The plane of the Earth equator cuts the celestial sphere in a great circle. This circle is the primary circle of the celestial sphere and is called the celestial equator. Extending the rotational axis of the Earth, it will intersect the celestial sphere at the north and south celestial poles.

Just like the meridians of longitude of the longitude-latitude system, meridians of right ascension (or hour circles) are secondary circles, each of which pass through both poles. Right ascension is measured from the celestial equator and has positive values towards the north celestial pole and negative values towards the south celestial pole.
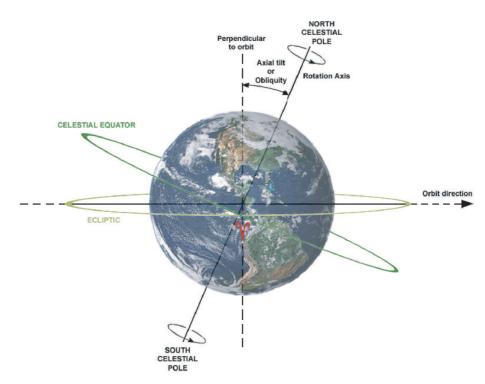
Figure 4: Illustration of the celestial equatorial system with reference to Earth and its orbit. The celestial equator is inclined at 23°27′ (Roy, 1988) to the ecliptic plane. The figure also indicates the position of the sun at the northern vernal equinox (♈). This figure is created by Dennis Nilsson and is licensed under the Creative Commons Attribution 3.0 Unported License (http://creativecommons.org/licenses/by/3.0/).

Parallels of declination are, just like parallels of latitude, small circles parallel to the celestial equator. Right ascension is measured eastwards either in degrees, or in hours, minutes and seconds of time. The Earth orbits the sun in what is known as the ecliptic plane and it intersects the celestial sphere in a great circle called the ecliptic. The Earth's rotational axis makes an angle of 23°27′ with the normal to the plane of ecliptic and is termed the obliquity of the ecliptic (ε). The point of zero right ascension is defined at one of the two nodes where the ecliptic plane intersects the celestial equator – at the one where the sun crosses the celestial equator from south to north. This point corresponds to the position of the sun at the northern vernal equinox (♈), also called the first point of Aries. Since the Earth rotates, the celestial equatorial system appears to rotate 360° each solar day, or in 24 h, in the westward direction as seen from the Earth surface. Thus, the relationship between measuring the right ascension in degrees or time is:

$$24^h = 360°. \tag{2}$$

Furthermore,

$$1^h = 15°, \qquad 1^m = 15', \qquad 1^s = 15'', \tag{3}$$

and

$$1° = 4^m, \qquad 1' = 4^s, \qquad 1'' = \frac{1}{15}^s. \tag{4}$$

A more exhaustive description of the celestial equatorial system can be found in any book on astronomy, e.g., Zeilik and Gregory (1998) and Green (1988).
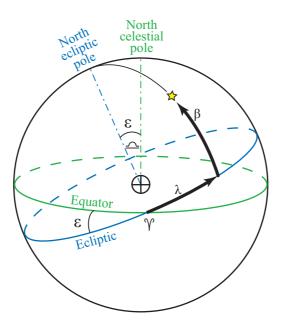
Figure 5: Sketch of the ecliptic system in reference to Earth ($\oplus$) and the Earth/celestial equator. The equator is inclined by $\varepsilon = 23°27'$ (Roy, 1988) to the ecliptic plane. The equator and the ecliptic plane cross at the northern vernal equinox (Υ) and the northern autumnal equinox ($\triangleq$). How to specify the ecliptic longitude (λ) and ecliptic (β) of an object is also indicated.

5.4   THE ECLIPTIC SYSTEM

The fundamental plane of reference of the ecliptic system is the plane of ecliptic, as is visualized in Figure 5. It intersects the celestial equator at two points, at the northern vernal equinox and the northern autumnal equinox ($\triangleq$). The poles of the ecliptic are defined where the normal to the ecliptic plane intersects the celestial sphere, at an angle equal to ε to the Earth rotational axis. The north ecliptic pole is the one located on the same side of the ecliptic as the north celestial pole.

At any instant, the sun lies in the ecliptic. Therefore, in addition to the diurnal motion of the sun, in one year it traces out the ecliptic as it moves eastwards about 1° per day as seen from Earth.

The quantities used to describe the position of a target is ecliptic longitude (λ) and latitude (β). The ecliptic longitude is the angular distance in the eastward direction from the vernal equinox (just like the right ascension) along the ecliptic to the point where a great circle through the poles of the ecliptic and the position of the object crosses the ecliptic. The ecliptic latitude is the angular distance along the same great circle from the ecliptic to the target. Ecliptic latitude is positive towards the north ecliptic pole and negative towards the south one.

In most cases, the origin of the ecliptic system is chosen to be either the center of the Earth or the center of the Sun. Here we only consider the center of the Earth as the origin.

A useful application of the ecliptic system, e.g., when plotting meteor radiants, is to subtract the ecliptic longitude of the sun (it is always located at $\beta = 0$) from the position of the target, putting the sun at $\lambda = 0$ for all observations. This is called the sun-centered longitude ($\lambda - \lambda_\odot$). The Sun is situated at 90° ecliptic longitude at summer solstice, at 180° at autumnal equinox and at 270° at winter solstice.

For more information, the reader may consult, e.g., Roy (1988) and Green (1988).
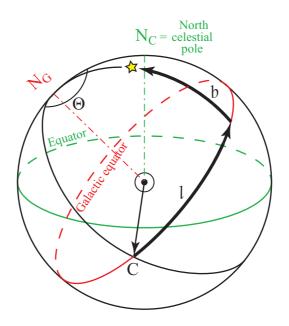
Figure 6: Sketch of the galactic system in reference to the ecliptic. The symbols and variables are: $\odot$ represents the sun, C is the direction of the galactic center as seen from the sun, N_C and N_G are the north celestial and the north galactic pole respectively, l and b are the the galactic longitude and latitude of an object and Θ is the angle between C and N_C.

5.5   THE GALACTIC SYSTEM

Describing positions and/or motions of stars or interstellar particles, the plane of the galaxy is a natural reference plane. At each end of the normal to this plane, we have a pole; the one on the same side of the galactic plane as the celestial north pole (N_C) is defined as the north galactic pole (N_G). The galactic plane cuts the celestial sphere in a great circle termed the galactic equator, as drawn in Figure 6. The galactic and the ecliptic equators meet in two nodes.

The galactic latitude (l) and the galactic longitude (b) are measured in the same manner as the geodetic latitude/longitude and the ecliptic latitude/longitude. The reference point of the galactic longitude is the direction to the center of the galaxy (C) from the sun ($\odot$), the sun being located at the origin of the galactic system.

To relate the equatorial coordinates and the galactic coordinates of the same celestial object, the right ascension and declination of N_G (α_G, δ_G) and the angle between C and N_C (Θ) must be known. It is important to stress that since the north celestial pole has a precessional movement (because it is aligned with the rotational axis of Earth), α_G, δ_G and Θ change and thus the epoch for which they apply has to be specified. The adopted values of the equatorial coordinates for N_G for the Julian year 2000 are (Cox, 2000)

$$
\begin{aligned}
\alpha_{N_G} &= 12^h 51^m 26^s 28 = 195.86°, \\
\delta_{N_G} &= +27°7'41''.70 = +27.13°, \\
\theta &= 122.93°.
\end{aligned}
\tag{5}
$$

More detailed descriptions on the galactic coordinates can be found in, e.g., Green (1988) and Roy (1988).

6 METHODOLOGY OF ORBIT CALCULATIONS

UR TRISTATIC EISCAT UHF data give us precise particle deceleration and radar cross section, which we have compared and fitted to a single-object numerical ablation model (Section 4.1). Orbit calculations start with the atmospheric entry velocity (V_∞) of the meteoroids obtained from the ablation model, the dates and times, zenith distance (zd) and azimuth (az) (Section 5.2) for the events as well as the coordinates of the common volume. The common volume of the transmitter and the two receiver antenna beams is located at geodetic latitude $\Phi = 68.88° \cdot \pi/180$ (radians) and western geodetic longitude $\Lambda = -21.88° \cdot \pi/180$ (radians). The code we have used in this section is based on a translation from a prototype procedure developed by D. D. Meisel. It has been tested on jointly-held data in cooperation with him. This code is an enhanced version of a radar meteor orbit calculation program synthesized from algorithms presented in Dubyago (1961), Danby (1988) and Wilkins and Springett (1977) under supervision of D. D. Meisel. Unreferenced details are obtained in personal communication with D. D. Meisel. The results are presented in Paper I. Details of the corrections and the method of calculation follow.

6.1 CORRECTING FOR THE FLATTENING AND ROTATION OF THE EARTH

The first effect we take into account when calculating the meteoroid orbits is the parallax due to the displacement of the observer from the centre of Earth. To do this, the flattening of the Earth (f) needs to be taken into account. It equals the relative difference between the equatorial and polar radius of the Earth and $f = 1/298.257$ (Seidelmann, 1992). The normalised distance from the center of the Earth to the ground projection of the common volume (in units of Earth equatorial radius) can be expressed as

$$\rho_{cv} = \sqrt{C^2 \cdot (\cos^2 \Phi + (1-f)^4 \cdot \sin^2 \Phi)} \tag{6}$$

(Wilkins and Springett, 1977), where Φ is the the geodetic latitude of the common volume and C is defined as

$$C = (\cos^2 \Phi + (1-f)^2 \cdot \sin^2 \Phi)^{-1/2} \tag{7}$$

(Wilkins and Springett, 1977). Then, the distance to the common volume (km) is

$$r_{cv} = \rho_{cv} \cdot R_\oplus + H, \tag{8}$$

where $R_\oplus$ is the equatorial radius (km) of the Earth and H is the height of the common volume (km). This is used to correct the meteoroid velocities for the Earth's rotation. To do that, we need to calculate how our observational point propagates eastwards with the Earth (V_{east}). The rotation rate of the Earth is

$$\omega_\oplus = 2\pi/sidereal\ day = 7.2921159 \cdot 10^{-5}\ \text{radians/s}, \tag{9}$$

thus
$$V_{east} = r_{cv} \cdot \omega_\oplus. \tag{10}$$

The Earth's velocity (km/s) along our line-of-sight, or trajectory, depends on the azimuth (az) and zenith distance (zd) of the observed meteoroid:

$$\Delta V = V_{east} \cdot \sin az \cdot \sin zd \cdot \cos \Phi. \tag{11}$$

Since we want to subtract the Earth's rotation from the observed meteoroid velocity (km/s) that has been integrated backwards up to the top of the atmosphere, the corrected velocity (km/s), i.e. the geocentric velocity, becomes

$$V_g = V_\infty - \Delta V. \tag{12}$$

6.2 SOLAR COORDINATES

The aim with the next few equations is to calculate the ecliptic longitude of the Earth's apex at the time of meteor detection. A way to do this is to consider the sun moving around the Earth in an elliptical orbit. The equations are taken from Wilkins and Springett (1977).

We start with the longitude of the sun (radians), $l_\odot$, for which we need the solar longitude of periapsis (degrees) (see Section 6.6 and 6.6.8)

$$\omega_\odot = 281.220844 + 1.719175 \cdot t_0 + 4.5277778 \cdot 10^{-4} \cdot t_0^2 + 3.333334 \cdot 10^{-6} \cdot t_0^3, \tag{13}$$

the mean anomaly of the sun (degrees)

$$m_\odot = 358.475833 + 35999.04975 \cdot t_0 - 1.5 \cdot 10^{-4} \cdot t_0^2 - 3.3 \cdot 10^{-6} \cdot t_0^3, \tag{14}$$

and the eccentricity of the sun's orbit (or in reality of the Earth's orbit)

$$e_\odot = e_\oplus = 0.01675104 - 0.00004180 \cdot t_0 - 0.0000000126 \cdot t_0^2. \tag{15}$$

In equations (13)-(15), t_0 is the number of Julian centuries of 36 525 days from the epoch of Dublin Julian Day (DJD) to the date of observation. The DJD epoch is noon UT 1900 January 0 (1899 December 31) and relates to the Julian Day (JD) as

$$DJD = JD - 2415020.0. \tag{16}$$

The longitude of the sun (radians) is calculated as

$$l_\odot = \left(\omega_\odot + m_\odot + 2 \cdot e_\odot \cdot \sin m_\odot + \frac{5 \cdot e_\odot^2 \cdot \sin 2m_\odot}{4} \right) \frac{\pi}{180}, \tag{17}$$

and is the position of the sun as seen from Earth, at At vernal equinox, $l_\odot = 0$.

Next we need the eccentric anomaly of the sun ($E_\odot$) "in orbit around Earth" (the concept of eccentric anomaly is discussed in Sections 6.6 and 6.6.5) and the solar distance ($r_\odot$) from the centre of the Earth. We can use the mean anomaly of the sun and the eccentricity to calculate both. The relation between $m_\odot$, $e_\odot$ and the eccentric anomaly ($E_\odot$) is:

$$E_\odot = m_\odot + e_\odot \cdot \sin E_\odot \tag{18}$$

(Murray and Dermott, 1999). The above equation can be solved iteratively for small values of the eccentricity ($e < 0.6627$), as explained by, e.g., Roy (1988). We have used the first three terms of the expansion in powers of $e_\odot$ to calculate the eccentric anomaly of the sun (radians):

$$E_\odot = m_\odot + \left(1 - \frac{e_\odot^2}{8} \right) \cdot e_\odot \cdot \sin m_\odot + \frac{e_\odot^2 \cdot \sin 2m_\odot}{2} + \frac{3 \cdot e_\odot^3 \cdot \sin 3m_\odot}{8}. \tag{19}$$

Knowing $E_\odot$, the solar distance (AU) from the centre of Earth is trivial:

$$r_\odot = a_\odot \cdot (1 - e_\odot \cdot \cos E) \tag{20}$$

(Murray and Dermott, 1999), where $a_\odot$ (AU) is the semi-major axis of the Earth's orbit around the sun. Both $E_\odot$ and $r_\odot$ are calculated at the time of the meteoroid detection. Then the velocity (km/s) of the sun in its orbit around the Earth is

$$v_{\odot x} = \frac{-29.784767}{r_\odot} \cdot \sin E_\odot \tag{21}$$

along the semi-major axis and

$$v_{\odot y} = \frac{29.784767}{r_\odot} \sqrt{1 - e_\odot} \cdot \cos E_\odot \tag{22}$$

along the minor axis. The number 29.784767 in equations (21) and (22) is the mean orbital speed of Earth (km/s) (Seidelmann, 1992). Thus the full solar velocity (km/s) is

$$v_\odot = \sqrt{v_{\odot x}^2 + v_{\odot y}^2}. \tag{23}$$

Now, if we switch from envisaging the sun from the Earth to looking at the Earth from the sun, the Earth's velocity will be of the same magnitude as the sun's velocity, but in the opposite direction. Consequently, by reversing the solar velocities, the velocities represent the Earth's velocity towards its apex and we can calculate the ecliptic longitude (radians) of the apex (Danby, 1988)

$$l_{apex} = \tan^{-1} \frac{-v_{\odot y}}{-v_{\odot x}} + \omega_\odot. \tag{24}$$

6.3 ABERRATION AND ZENITH ATTRACTION CORRECTION

Before we continue with more corrections, we need to calculate some quantities. First we convert the zenith distance (zd, radians) to altitude (alt, radians)

$$alt = \frac{\pi}{2} - zd, \tag{25}$$

as explained in Section 5.2. Then we calculate the Greenwich mean sidereal time (degrees) at 0h UT

$$\theta_G = 100.46061837 + 36000.770053608 \cdot t + 0.000387933 \cdot t^2, \tag{26}$$

where t is the number of Julian centuries of 36 525 days from the epoch J2000.0 to the date of observation. The J2000.0 epoch is 2000 January 1, 11:58:55.816 UTC and is related to the Julian Day (JD) as

$$DJD = JD - 2451545.0 \tag{27}$$

(compare with Equation (16)). To calculate the Greenwich mean sidereal time for the time of detection, θ_G needs to be corrected by the time of day

$$\theta_1 = \theta_G + (hour \cdot 15.041 + min \cdot 0.25068 \cdot sec \cdot 0.0041781) \cdot 1.0027337909 \tag{28}$$

and converted into radians. Earth rotates $360°$ each sidereal day, i.e., each $23^h56^m4.09054^s$. Thus Earth rotates $15.041°$ per hour, $0.25068°$ per minute and $0.0041781°$ per second. Since our times are given in mean solar days, we need to multiply by 1.0027337909, the length of a mean sidereal day expressed in mean solar days (Seidelmann, 1992; Danby, 1988).

Next we need to convert the altitude and azimuth to hour angle (h), right ascension (α) and declination (δ). The celestial equatorial system is described in Section 5.3. The formulae connecting these coordinates can be thought of as correction cosines and are:

$$c_X = \cos\delta \cdot \cos h = \quad \cos\Phi \cdot \sin alt - \sin\Phi \cdot \cos alt \cdot \cos az, \tag{29}$$

$$c_Y = \cos\delta \cdot \sin h = -\cos alt \cdot \sin az, \tag{30}$$

and

$$c_Z = \sin\delta \qquad = \quad \sin\Phi \cdot \sin alt + \cos\Phi \cdot \cos alt \cdot \cos az \tag{31}$$

(Wilkins and Springett, 1977). Evidently, the hour angle (radians) is given by

$$h = \tan^{-1}\frac{c_Y}{c_X} \tag{32}$$

and the declination (radians) by

$$\delta = \sin^{-1} c_Z. \tag{33}$$

The right ascension (radians) is obtained from the equation

$$\alpha = local\ sidereal\ time - h = \theta_1 - \Lambda - h, \tag{34}$$

where $\Lambda = -21.88° \cdot \pi/180$ (radians) is the geodetic western hemisphere longitude (see Section 5.1) of the common volume.

However, the position of the radiant of the observed meteoroid depends on the motion of the observer. The observer is in this case is the measurement volume and it moves with the rotational velocity of Earth. This causes an effect similar to the diurnal aberration of celestial bodies (Dubyago, 1961) and depends on the time of observation as well as the position of the observer. By changing the velocity of light for the velocity of the meteor in the formulae for diurnal aberration, the correction in right ascension (radians) and declination (radians) can be obtained (Dubyago, 1961) from

$$\Delta\alpha = -\frac{2\cdot\pi\cdot r_{cv}}{86164.09054}\cdot\frac{1}{V_g\cdot\cos\delta}\cdot\cos\phi\cdot\cos h, \tag{35}$$

$$\Delta\delta = -\frac{2\cdot\pi\cdot r_{cv}}{86164.09054}\cdot\frac{1}{V_g}\cdot\frac{\pi}{180}\cdot\cos\phi\cdot\sin h\cdot\sin\delta, \tag{36}$$

where the number 86 164.090 54 is a sidereal day in seconds and ϕ is the geocentric latitude (described in Section 5.1) of the common volume and is given by

$$\phi = \tan^{-1}\left(\left(1 - f^2\right)\tan\Phi\right). \tag{37}$$

Thus the values corrected for aberration, indicated with subscript 1, are

$$\alpha_1 = \alpha + \Delta\alpha \tag{38}$$

and

$$\delta_1 = \delta + \Delta\delta. \tag{39}$$

Now we can convert the right ascension and declination back to zenith distance and azimuth to perform the zenith attraction correction before we once again go back to right ascension and declination. To begin with, we need to calculate the corrected hour angle (radians)

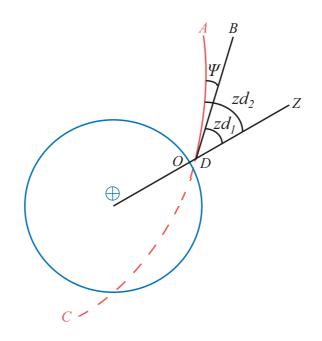$$h_1 = \theta_G - \Lambda - \alpha_1. \tag{40}$$

Figure 7: Illustration of the zenith attraction. The blue circle is Earth. The meteoroid comes in on a hyperbolic trajectory ADC. The meteor is detected at point D, for simplicity in the direction of the observer's zenith, Z. The observer is observing from point O. When detecting a meteor, we see it coming from the tangent BD to its actual orbit. Thus the zenith distance measured is zd_1 while the real zenith distance is zd_2. From the figure it is evident that $zd_1 < zd_2$ and the difference is the angle Ψ. This figure is inspired by the drawing of the zenith attraction in Dubyago (1961).

The conversion cosines are:

$$c_{X_1} = \cos alt \cdot \cos az = \quad \sin \delta_1 \cdot \cos \phi - \cos \delta_1 \cdot \cos h_1 \cdot \sin \phi, \tag{41}$$

$$c_{Y_1} = \cos alt \cdot \sin az = - \cos \delta_1 \cdot \sin h_1, \tag{42}$$

$$c_{Z_1} = \sin alt \qquad = \quad \sin \delta_1 \cdot \sin \phi + \cos \delta_1 \cdot \cos h_1 \cdot \cos \phi, \tag{43}$$

where ϕ (radians) is the corresponding latitude to Φ if the Earth was spherical. The corrected altitude (radians) is easily calculated as

$$alt_1 = \sin^{-1} c_{Z_1}, \tag{44}$$

which gives the corrected zenith distance (radians) as

$$zd_1 = \frac{\pi}{2} - alt_1. \tag{45}$$

A meteor seems to come from a more vertical direction, with a smaller zenith distance, than it actually does. The reason for this is Earth's gravity, which, makes the particle bend towards the center of the Earth. What we measure is thus the tangent to the meteoroid's curved path at our location (Dubyago, 1961). This effect is called zenith attraction, or hyperbolic attraction of the Earth, and is illustrated in Figure 7. Also, the hyperbolic attraction of the Earth will accelerate the meteoroid. According to Dubyago (1961) the corrected velocity (km/s) is calculated as

$$V_2 = \sqrt{V_g^2 - 2 \cdot g \cdot r_{cv}}, \tag{46}$$

where V_g (km/s) is the geocentric velocity of the meteoroid, i.e., the meteoroid velocity corrected for the Earth's rotation (eq. (12)), ρ_{cv} (km) is the normalized distance from

the centre of the Earth to the ground projection of the common volume (eq. (6)) and g (km/s^2) is the strength of the Earth's gravity field at the common volume. The acceleration of gravity is given by the universal law of gravitation combined with Newton's second law (km/s):

$$g = G \frac{M_\oplus}{r_{cv}^2}, \tag{47}$$

where G is the gravitational constant of the universe expressed in km^{3}kg^{-1}s^{-2} and $M_\oplus$ is the mass of Earth (kg). The correction angle Ψ (radians) for the zenith distance is derived in Dubyago (1961):

$$\tan \frac{1}{2} \Psi = \frac{V_g - V_2}{V_g + V_2} \cdot \tan \frac{zd_1}{2}. \tag{48}$$

Rearranging equation (48) for Ψ,

$$\Psi = 2 \cdot \tan^{-1} \frac{V_g - V_2}{V_g + V_2} \cdot \tan \frac{zd_1}{2}. \tag{49}$$

The radiant position corrected for aberration and zenith attraction is indicated with subscript 2 and is

$$az_2 = \tan^{-1} \frac{c_{Y_1}}{c_{X_1}}, \tag{50}$$

$$zd_2 = zd_1 + \Psi, \tag{51}$$

and

$$alt_2 = \frac{\pi}{2} - zd_2. \tag{52}$$

Equations (29), (30) and (31) are useful again, but with az_2, alt_2 and ϕ instead of az, alt and Φ respectively, when converting the new radiant position back to right ascension and declination. Then,

$$h_2 = \tan^{-1} \frac{c_Y}{c_X}, \tag{53}$$

$$\alpha_2 = \theta_1 - \Lambda - h_2, \tag{54}$$

and

$$\delta_2 = \sin^{-1} c_Z. \tag{55}$$

6.4   ECLIPTIC RADIANT

We are now ready to transform the geocentric radiant into ecliptic coordinates, which are presented in Section 5.4. The conversion equations from right ascension and declination to ecliptic longitude, λ (radians), and latitude, β (radians), are

$$c_{X_2} = \cos \beta \cdot \cos \lambda = \cos \delta_2 \cdot \cos \alpha_2, \tag{56}$$

$$c_{Y_2} = \cos \beta \cdot \sin \lambda = \sin \varepsilon \cdot \sin \delta_2 + \cos \varepsilon \cdot \cos \delta_2 \cdot \sin \alpha_2, \tag{57}$$

and

$$c_{Z_2} = \sin \beta \qquad = \cos \varepsilon \cdot \sin \delta_2 - \sin \varepsilon \cdot \cos \delta_2 \cdot \sin \alpha_2, \tag{58}$$

where ε (radians) is the obliquity of the ecliptic, i.e., the angle between the ecliptic plane and the Earth's orbital plane around the sun (Wilkins and Springett, 1977). This angle has the form

$$\varepsilon = \left(23.452 - 0.01301 \cdot t_0 - 1.64 \cdot 10^{-6} \cdot t_0^2 + 5.03 \cdot 10^{-7} \cdot t_0^3\right) \frac{\pi}{180}, \tag{59}$$

where t_0 is described in Section 6.2 (Wilkins and Springett, 1977). The long time variation of ε is due to the Earth axis precession and is about $1°$ in 100 000 years. Equations (56)-(58) give

$$\lambda = \tan^{-1} \frac{c_{Y_2}}{c_{X_2}}, \tag{60}$$

and

$$\beta = \sin^{-1} c_{Z_2}, \tag{61}$$

and are the ecliptic coordinates of the radiant of the meteoroid in the Earth's frame of reference, i.e., where the meteoroid is coming from. The sun-centered ecliptic longitude (radians) of the meteor radiant with geocentric velocity (Earth's velocity not subtracted) can now be calculated:

$$\lambda_\odot = \lambda - \left(l_{apex} + \frac{\pi}{2}\right). \tag{62}$$

The ecliptic longitude of the sun is always located $+\frac{\pi}{2}$ from the ecliptic longitude of the apex and consequently, $+\frac{\pi}{2}$ needs to be added to it.

6.5   TRUE HELIOCENTRIC RADIANT

Next we have to calculate the true heliocentric radiant, in other words subtracting the orbital velocity of the Earth. This is done through a set of auxiliary angles n, γ and N adopted from Dubyago (1961). To begin with, the coordinates relative to the apex have the following relationship

$$d_{X_1} = \sin n \cdot \cos \gamma = \sin(\lambda - l_{apex}) \cdot \cos \beta, \tag{63}$$
$$d_{Y_1} = \sin n \cdot \sin \gamma = \sin \beta, \tag{64}$$

and

$$d_{Z_1} = \cos n \qquad = \cos(\lambda - l_{apex}) \cdot \cos \beta. \tag{65}$$

These directions can be thought of as a coordinate system rotating with and centered at Earth with the x axis pointing towards the sun, the y axis towards the North Ecliptic Pole (NEP) and the z axis towards the apex. Solving for γ, we get

$$\gamma = \tan^{-1} \frac{d_{Y_1}}{d_{X_1}}. \tag{66}$$

This angle tells us where the meteor radiant is located with respect to the ecliptic, i.e., the angle between the ecliptic and the meteoroid radiant projected onto the xy plane. Then, the component of the radiant direction perpendicular to the apex direction can be determined as

$$d_Q = \frac{d_{Y_1}}{\sin \gamma}, \tag{67}$$

and the angle between the meteor radiant and the apex as

$$n = \tan^{-1} \frac{d_Q}{d_Z}. \tag{68}$$

Using n, we can subtract the Earth's velocity from the meteoroid velocity, i.e., correct it for heliocentric velocities, to obtain the meteoroid heliocentric velocity V_h:

$$V_h = \sqrt{V_2^2 + v_\odot^2 - 2 \cdot V_2 \cdot v_\odot \cdot \cos n}. \tag{69}$$

Next we need to determine the angle N between the heliocentric velocity of Earth ($V_\odot$) and the heliocentric velocity of the meteoroid (V_h):

$$\sin(N - n) = \frac{v_\odot}{V_h} \sin n$$

$$N = \sin^{-1}\left(\frac{v_\odot}{V_h} \sin n\right) + n. \tag{70}$$

Subtracting the Earth's velocity means that we stop the d_{X_1}, d_{Y_1} and d_{Z_1} coordinate system from rotating and fixing it at the instance where the meteoroid was detected. Switching n to N in equation (63)-(65), we get the relationships

$$d_{Y_2} = \sin N \cdot \cos\gamma = \sin(\lambda_0 - l_{apex}) \cdot \cos\beta_0, \tag{71}$$

$$d_{Z_2} = \sin N \cdot \sin\gamma = \sin\beta_0, \tag{72}$$

and

$$d_{X_2} = \cos N \qquad = \cos(\lambda_0 - l_{apex}) \cdot \cos\beta_0. \tag{73}$$

where d_{X_2} points towards the apex, d_{Y_2} towards the sun and d_{Z_2} towards NEP and β_0 (radians) and λ_0 (radians) are the true ecliptic coordinates of the heliocentric velocity at Earth, which is the same as the direction of the radiant. Equations (73)-(72) give

$$\beta_0 = \sin^{-1} d_{Z_2}, \tag{74}$$

and

$$\lambda_0 = \tan^{-1}\frac{d_{Y_2}}{d_{X_2}} + l_{apex}. \tag{75}$$

6.6   ORBITAL ELEMENTS

A standard way of specifying an orbit uniquely is to use a set of six orbital elements called Keplerian elements. These are inclination (i), longitude of the ascending node (Ω), arguments of perihelion (ω), eccentricity (e), semi-major axis (a) and true anomaly (ν). Some of the orbital elements are sketched in Figure 8.

The inclination describes the tilt of the orbital plane. It is the angular distance of the orbital plane from the plane of reference, in this case the ecliptic. Orbits with $0° \leq i < 90°$ are prograde while orbits with $90° < i \leq 180°$ are retrograde. If an orbit has an $i \neq 0$, then it has two nodes. The two nodes of an orbit are the points where the orbital plane crosses the plane of reference to which it is inclined. The ascending node (Ω) is the node at which the celestial body moves from below to above its plane of reference; the descending node ($\mho$) is the opposite point. The longitude of the ascending node is then the angle from a reference direction to the direction of the ascending node, measured in the reference plane.

The argument of perihelion is the angle from the ascending node, measured in the orbital plane, to the periapsis, which in our case, when the sun is the central body, is the same as the perihelion. The eccentricity describes the shape of the orbit: $e = 0$ for circular orbits, $0 < e < 1$ for elliptic orbits, $e = 1$ for parabolic trajectories and $e > 1$ for hyperbolic orbits. The size of the orbit is determined by the semi-major axis.

For our purposes, we have determined some of the orbital elements described above and some others relevant for this work.
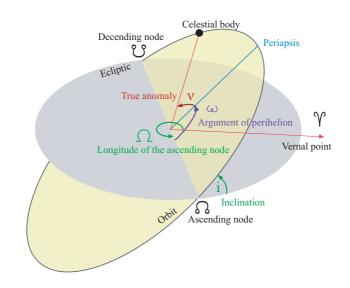
Figure 8: Plot showing the orbital elements and more for an orbital plane inclined to the ecliptic. This figure is created by Árpád Horváth and is licensed under the Creative Commons Attribution ShareAlike 2.5 License (http://creativecommons.org/licenses/by-sa/2.5/).

6.6.1 INCLINATION

The inclination can be calculated as the angle between the normal to the orbital plane, i.e., the direction of the angular momentum, and the normal to the reference plane, in our case the z axis, which points towards NEP (eq. (72)). Thus the magnitude of the cosine (along the z axis) and the sine (in the ecliptic plane) components of the angular momentum is (Dubyago, 1961):

$$c_L = r_\odot \cdot V_h \cdot \cos \beta_0 \cdot \sin(\lambda_0 - l_\odot), \tag{76}$$

$$s_L = r_\odot \cdot V_h \cdot |\sin \beta_0|. \tag{77}$$

The angular momentum is then given by Pythagoras' theorem:

$$L = \sqrt{c_L^2 + s_L^2}. \tag{78}$$

The inclination (radians) of the angular momentum is now easily obtained:

$$i = \cos^{-1} \frac{c_L}{L}. \tag{79}$$

6.6.2 SEMI-MAJOR AXIS

The semi-major axis (see Figure 9) of the meteoroid orbit (a) can be obtained directly in AU from (Dubyago, 1961)

$$\frac{1}{a} = \frac{2}{r_\odot} - V_h^2, \tag{80}$$

if the meteoroid orbital velocity is multiplied with the quantity

$$\frac{D \cdot 1000}{k \cdot AU}, \tag{81}$$

where D is the mean solar day in seconds (86 400 s), $k = 0.01720209895 \text{ AU}^{3/2} \text{m}_\odot^{-1/2} \text{D}^{-1}$ is the Gaussian gravitational constant and AU is one astronomical unit expressed in m. The Gaussian gravitational constant is the gravitational constant of the universe, G, expressed in units of the solar system rather than SI units.
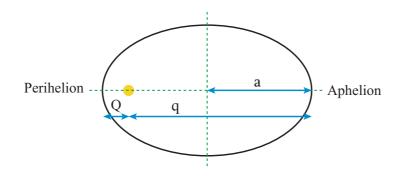
Figure 9: Sketch of the perihelion distance (Q), the aphelion distance (q) and the semi-major axis (a) of an ellipse.

6.6.3   ECCENTRICITY

According to Dubyago (1961), the eccentricity of the meteoroid orbits can be calculated from the equations

$$s_\nu = e \cdot \sin \nu = \frac{L \cdot \cos i}{r_\odot \cdot \tan(\lambda_0 - l_\odot)}, \tag{82}$$

and

$$c_\nu = e \cdot \cos \nu = \frac{L}{r_\odot} - 1, \tag{83}$$

$$\tag{84}$$

where ν is the true anomaly. We will deal with ν later (Section 6.5). The eccentricity is obtained by squaring equations (82) and (83) and then adding them together:

$$\begin{aligned} e^2 \cdot \sin^2 \nu + e^2 \cdot \cos^2 \nu &= s_\nu^2 + c_\nu^2 \\ e^2(\sin^2 \nu + \cos^2 \nu) &= s_\nu^2 + c_\nu^2 \\ e^2 &= s_\nu^2 + c_\nu^2 \\ e &= \sqrt{(s_\nu^2 + c_\nu^2)}. \end{aligned} \tag{85}$$

6.6.4   PERIHELION AND APHELION DISTANCE

In the case of an elliptical orbit around the sun, perihelion is the point in the orbit that is closest to the sun and aphelion is the point farthest from the sun, as illustrated in Figure 9. A hyperbolic orbit has only a perihelion and no aphelion. The perihelion (Q) and the aphelion distance (q) are the shortest and largest distances between the foci and the ellipse respectively. In a circular orbit, Q, q and a are all the same, namely equal to the radius.

Both quantities are easily calculated when we already know the semi-major axis (a) and the eccentricity (e) of the orbits (eq. (80), (85); Dubyago (1961)),

$$Q = a \cdot (1 - e), \tag{86}$$
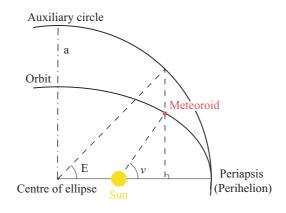$$q = a \cdot (1 + e). \tag{87}$$

Figure 10: Illustration of the true (ν) and the eccentric anomaly (E).

6.6.5 TRUE AND ECCENTRIC ANOMALY

The next two quantities to be determined are the true and the eccentric anomaly; both are drawn in Figure 10. The true anomaly (ν) is the angle between the direction of perihelion and the position of the meteoroid in its orbit, as seen from the sun (Danby, 1988). To describe the eccentric anomaly (E) we need to draw a reference circle around the orbital ellipse with radius a. The eccentric anomaly is then the angle between the direction of perihelion and the position of the meteoroid projected onto the auxiliary circle by a perpendicular to the semi-major axis through the true position of the meteoroid, as seen from the centre of the ellipse.

If we go back to Section 6.6.3, equations (82) and (83) contain ν (radians), and it is time to take advantage of that. Dividing equation (82) with (83), we get

$$\nu = \tan^{-1} \frac{s_\nu}{c_\nu}. \tag{88}$$

The relation between ν and E (radians) is (Murray and Dermott, 1999)

$$\tan \frac{\nu}{2} = \sqrt{\left(\frac{1+e}{1-e} \right)} \cdot \tan \frac{E}{2}. \tag{89}$$

Solving equation (89) for E,

$$E = 2 \cdot \tan^{-1} \left(\tan \frac{\nu}{2} \cdot \sqrt{\left(\frac{1-e}{1+e} \right)} \right). \tag{90}$$

6.6.6 TIME FROM PERIHELION

Time from perihelion (Δt) is, as the name indicates, the time in days from the particle's perihelion passage to detection. A positive Δt means a postperihelion particle, while a negative Δt means a preperihelion particle. An equation for calculating the time from perihelion is derived in Dubyago (1961) and solving for Δt gives

$$\Delta t = \frac{|a|^{2/3}}{k} \left(E - e \cdot \sin E \right). \tag{91}$$

The reason for taking the absolute value of the semi-major axis is that it is negative for hyperbolic orbits and thus would result in the wrong sign on the time from perihelion.

6.6.7   LONGITUDE OF THE ASCENDING NODE

Since the Earth's orbit is in the ecliptic, we only observe meteoroids when they are either at their ascending (☊) or descending node (☋), i.e., when they cross the ecliptic in their orbit. To clarify, if we detect a particle coming from the equator, we detect it at its ascending node, if it comes from the direction of the pole, we detect it at its descending node. For illustration, see Figure 8.

The longitude of the ascending node (Ω) equals the ecliptic longitude of the sun ($l_\odot$, eq. (17)) as seen from the Earth if the meteoroid is detected at its descending node, that is when the meteor radiant is located at positive ecliptic latitude, $\beta_0 > 0$ (eq. (74)). However, if $\beta_0 < 0$, then the meteoroid is at its ascending node instead and Ω is the ecliptic longitude of the sun $+\pi$ term. This is because the longitude of the sun is seen from the Earth while the longitude of the ascending node is seen from the sun. When the meteoroid is in its ascending node, then the two directions are opposite to each other, thus the $+\pi$. When the meteoroid is in its descending node, then the direction to the ascending node is in the same direction from both the sun and the Earth.

Finally, the equation for the longitude of the ascending node (radians) is:

$$\Omega = l_\odot + \left(1 - \frac{\beta_0}{|\beta 0|}\right) \cdot \frac{\pi}{2}. \tag{92}$$

6.6.8   ARGUMENT OF PERIHELION

The argument of perihelion, or periapsis, is the angle between the ascending node and perihelion in the orbital plane as seen from the sun. Since we observe the meteoroids either in their ascending or descending node (see Section 6.6.7), we know that if we add the argument of perihelion (ω) and the true anomaly (ν, eq. (88)) we get either π or 2π. Therefore, if we detect the meteoroid in its descending node ($\beta_0 > 0$, eq. (74)), then $\omega = 2\pi - \nu - \pi = \pi - \nu$. If we detected it in its ascending node instead ($\beta_0 < 0$), $\omega = 2\pi - \nu$, which is the same as $-\nu$ if we keep the argument of perihelion within $0 \leq \omega \leq 2\pi$. Thus we can calculate the argument of perihelion (radians) using β_0 to know which of the two cases we have:

$$\omega = \left(\frac{\beta_0}{|\beta_0|} + 1\right) \cdot \frac{\pi}{2} - \nu. \tag{93}$$

6.6.9   PERIOD

The orbital period (T) in seconds for a small body orbiting a central body is determined by the equation (Danby, 1988)

$$T = 2\pi\sqrt{\frac{a^3}{G \cdot M}}, \tag{94}$$

where G is the gravitational constant of the universe and M is the mass of the central body. Conveniently enough, if T is measured in years, a is expressed in AU and the central body is the sun, the period can be obtained extremely easily:

$$T = \sqrt{a^3} \tag{95}$$

(Danby, 1988). Intuitively, the orbital period can only be calculated for bound orbits.

7   Summary of the Included Papers

7.1   Paper I: Orbit Characteristics of the Tristatic EISCAT UHF Meteors

The observed velocities of the 410 tristatic EISCAT UHF meteors (see Section 4.1) are integrated back through the Earth's atmosphere to find their atmospheric entry velocities. The integration is performed using an ablation model, the particulars of which are outlined in Paper II and described in detail by Kero (2008). From the entry velocities, meteoroid orbits are calculated according to the description in Section 6. The results are presented in the form of different orbital characteristics.

None of the observed meteors are of clear interstellar origin; comets, particularly short period (< 200 years) ones, may be the dominant source for the particles observed. Almost half of the EISCAT UHF meteors are observed to radiate from the direction of the Earth apex. Furthermore, 58% of the orbits are retrograde. Only 33 orbits (8%) have an inclination $< 30°$, but their locations in the a/e diagram indicate that it is unlikely that any of them are of asteroidal origin.

The location of the EISCAT UHF system close to the Arctic Circle means that the North Ecliptic Pole (NEP) is near zenith once every 24 h, i.e., during each observational period. The meteoroid influx when NEP passes close to zenith should therefore be directly comparable throughout the year. Considering only the hour when NEP is closest to zenith, the EISCAT UHF head echo rate is about a factor of three higher at summer solstice than during the other observing periods.

7.2   Paper II: Estimated Visual Magnitudes of the EISCAT UHF Meteors

The purpose of the study presented in this paper was to investigate the requisites and suitable conditions for simultaneous meteor observations with telescopic optical devices and the EISCAT UHF system. Simultaneous high-resolution optical and radar observations of meteors are of great importance for the further understanding of the meteoroid-atmosphere interaction processes and the physics of the head echo.

The absolute visual magnitudes of the EISCAT UHF meteors are shown to be in the range of +9 to +5 and should be observable using intensified CCD or EMCCD (Electron Multiplying CCD) cameras with telephoto lenses.

Because of the general problem of interference from the high-power transmitter equipment on the optical instruments, the Tromsø site is an inappropriate camera location. In the paper we propose to use two cameras, one collocated with the Kiruna receiver to enable direct comparisons between radar and optical observations and a second one located in Kilpisjärvi, Finland, at 69.02°N and 20.86°E, providing a good complement to observations made in Kiruna. The elevation angle to the common volume is 65° and the azimuth makes almost a right angle with the Kiruna site azimuth.

As the EISCAT UHF system is located above the Arctic Circle, it is proposed that this study should be scheduled around or after autumnal equinox and when the moon is close to new.

7.2.1 FURTHER COMMENTS

The study suggested in Paper II was achieved in October 2007 as a joint campaign between IRF (the Swedish Institute of Space Physics) and the UWO (University of Western Ontario) Meteor Group providing two telescopic optical devices with telephoto lenses. One of the cameras was positioned in Kiruna, the other one in Peera, Finland, at 68.89°N and 21.06°E, about 20 km from Kilpisjärvi. The reason for the change of location was that the available site in Kilpisjärvi suffers from light pollution from the main road. The observation campaign resulted in 5 meteors observed with all three EISCAT UHF receivers and both cameras. The results will be presented in a future paper.

7.3 PAPER III: LATITUDINAL VARIATIONS OF DIURNAL METEOR RATES

This paper investigates diurnal meteor rate differences at different latitudes using specular meteor radar measurements from Esrange, Kiruna, Sweden, at 68°N; from Juliusruh, Germany, at 55°N; and from Ascension Island, at 8°S.

Radars at different latitudes see different sporadic meteor sources. The sources vary with season because of the tilt of the Earth axis. Thus the diurnal meteor event rate is found to differ between latitudes, with a larger seasonal variation at higher latitudes. The largest difference in amplitude of the diurnal flux variation (from morning to evening) is at equatorial latitudes and it is almost the same throughout the year. The lowest diurnal flux variation is found at polar latitudes, where the observations presented in this paper show the highest degree of seasonal variation of the diurnal flux.

7.4 PAPER IV: RADAR STUDIES OF THE SPORADIC METEOROID COMPLEX

This paper reports on sporadic meteor radiant distributions at high-, mid- and equatorial latitudes for different parts of the day at vernal/autumnal equinox and summer/winter solstice. Data used is collected by three specular meteor radars. The investigation shows a variation in the sources with both latitude and time of day. The paper also provides a review of how radiants for specular meteor trail detections are statistically determined.

Preliminary results are presented from the 2004 winter solstice EISCAT UHF campaign. The 47 observed tristatic meteors have geocentric velocities between about 15 and 67 km/s.

7.4.1 FURTHER COMMENTS

It should be noted that by methods described in Section 4.1, an additional number of 18 tristatic meteors have been found in the winter solstice data since the publication of this paper, which are included in later results (Papers I and II).

7.5   PAPER V: QUANTITATIVE COMPARISON OF A NEW AB INITIO MICROMETEOR ABLATION MODEL

An *ab initio* meteor ablation model has been constructed for the mass range 10^{-16} to 10^{-7} kg, devised for meteor head echo detections with the Arecibo Observatory 430 MHz UHF radar (AO). The faint end of this range cannot be observed by any other method, thus observational verification of the model is not possible. On the other hand, the EISCAT UHF system detects micrometeors in the high mass part of this range, is fitted to a standard ablation model and is observationally confirmable, as described in Paper II. The current paper presents a preliminary comparison of the *ab initio* and the standard model.

The largest difference between the two models is that the *ab initio* one uses mostly experimentally-determined data – for the heat transfer, thermal emissivity, the most important meteoroid elements and their oxides, as well as luminosity efficiency – which is the reason why we call it an *ab initio* model.

The initial and preliminary comparison of the two models show that the *ab initio* model will provide a useful extension of meteor ablation theory to the majority of the AO detected micrometeoroids. Further two model comparisons will be useful to understand any comprehensive comparison between the EISCAT and AO radar data.

Acknowledgements

At the beginning of time, when I started my PhD studies, the time span of five years felt never-ending. Yet the weeks added up to months, the months to years and here I am. I have gained a lot of knowledge, insight and understanding, not only in research but also in life and about myself. However, this thesis would never have been written without the help of others.

First of all, I would like to thank my supervisor Asta Pellinen-Wannberg for giving me the opportunity to dive into the field of meteors and the surroundings of Kiruna. Without the early work of Asta, Gudmund Wannberg, Assar Westman and Ingemar Häggström, this thesis would not exist.

This research work has been financed by the Swedish National Graduate School of Space Technology and the Swedish Institute of Space Physics. I am most thankful for this privilege. I am also indebted to Zonta International for supporting me through the Zonta International Amelia Earhart Fellowship.

David D. Meisel has played a very important role during the course of my work. With his passion for science and good humor he has taught me a great deal about what research is all about. And how to exercise it in practice.

My work would have been much more trying without my neighbours on the fourth floor: Johan Kero, Jonas Ekeberg, Martin Waara, Tony Giang, Andreas Ekenbäck, David McCann, Alla Belova, Daria Mikhaylova, Ella Carlsson, Alexander Grigoriev and Maria Smirnova. You have made me come out the other end smiling. I have really enjoyed being a member of "doktoranderna". Thank you!

Radar is not the only method I have used to observe meteors. I have also photographed meteors with the Auroral Large Imaging System (ALIS) under the guidance of Urban Brändström. He has been on duty many a night and patiently helped me through loads of camera crashes and other difficulties. Urban has been a great guru in many ways.

During EISCAT experiments, the staff at all three sites have been most obliging. I would especially like to give sincere thanks to Lars-Göran Vanhainen and Peter Bergqvist in Kiruna for offering their help anytime it was needed. Also Markku Postila and Jussi Markkanen in Sodankylä deserve many thanks for having done everything in their power to make the experiments run as smoothly as possible during my stays at the Sodankylä site.

Being a part of the research programme for Solar System Physics and Space Technology has meant a lot to me. I would like to acknowledge Stas Barabash for his efforts in creating a strong cohesive group; it really makes a difference.

My language skills are not as good as you might think, I have had great help with the quality of the text in this thesis from Rick McGregor. He has done a great job improving it, for which I am grateful.

The printing of this thesis would have been a pain without Torbjörn Lövgren. I really appreciate his devotion.

Also Carina Gunillasson and Stefan Vanhaniemi deserve my sincere gratitude for all their help during these years. They are always smiling no matter the whimsical nature of my demands and they never see problems, only solutions. I would also like to thank Vesa Alatalo for taking the well-being of the IRF staff seriously. I have done my best to take advantage of that.

There are not enough words to thank everyone who has been involved in the work on this thesis. I would like to thank everyone at IRF Kiruna for five wonderful, but also toilsome, years.

To my fantastic family and all my incredible friends: I would not be here, or anywhere close for that matter, if it weren't for you.

Johan, du är bäst!

REFERENCES

Baggaley, W. J., Bennett, R. G. T., Steel, D. I., and Taylor, A. D. (1994). The Advanced Meteor Orbit Radar facility - AMOR. *Quarterly Journal of the Royal Astronomical Society*, 35:293–320.

Beech, M. and Steel, D. (1995). On the definition of the term 'meteoroid'. *Quarterly Journal of the Royal Astronomical Society*, 36:281–284.

Bronshten, V. A. (1983). *Physics of meteoric phenomena*. D. Reidel Publishing Company.

Brownlee, D. E. (1985). Cosmic dust: collection and research. *Annual Review of Earth and Planetary Physics*, 13:147–173.

Campbell-Brown, M. D. (2007). Directional variation of sporadic meteor activity and velocity. *Earth, Moon, and Planets*. doi:10.1007/s11038-007-9152-8.

Ceplecha, Z., Borovička, J., Elford, W. G., ReVelle, D. O., Hawkes, R. L., Porubčan, V., and Šimek, M. (1998). Meteor phenomena and bodies. *Space Science Reviews*, 84:327–471.

Close, S., Brown, P., Campbell-Brown, M., Oppenheim, M., and Colestock, P. (2007). Meteor head echo radar data: Mass velocity selection effects. *Icarus*, 186:547–556.

Cox, A. N., editor (2000). *Allen's astrophysical quantities*. AIP and Springer, 4 edition.

Danby, J. M. A. (1988). *Fundamentals of celestial mechanics*. Willmann-Bell, 2nd. rev. and enlarged edition.

Dubyago, A. D. (1961). *The determination of orbits*. New York, Macmillan. Translated from Russion by R. D. Burke.

Evans, J. V. (1965). Radio-echo studies of meteors at 68-centimeter wavelength. *Journal of Geophysical Research*, 70:5395–5416.

Evans, J. V. (1966). Radar observations of meteor deceleration. *Journal of Geophysical Research*, 71:171–188.

Galligan, D. P. and Baggaley, W. J. (2004). The orbital distribution of radar-detected meteoroids of the solar system dust cloud. *Monthly Notices of the Royal Astronomical Society*, 353:422–446.

Genge, M. J. (2008). Micrometeorites and their implications for meteors. *Earth, Moon, and Planets*, 102:525–535.

Green, R. M. (1988). *Spherical astronomy*. Cambridge University Press, Great Britain.

Hawkes, R. L. (2002). *Meteors in the Earth's atmosphere*, Chapter: Detection and analysis procedures for visual, photographic and image intensified CCD meteor observations, pages 97–122. Cambridge University Press, Cambridge, UK.

Hedin, A. E. (1991). Extension of the MSIS thermosphere model into the middle and lower atmosphere. *Journal of Geophysical Research*, 96:1159–1172.

Herlofson, N. (1951). Plasma resonance in ionospheric irregularities. *Arkiv för fysik*, 3(15):247–297.

Hocking, W. K., Fuller, B., and Vandepeer, B. (2001). Real-time determination of meteor-related parameters utilizing modern digital technology. *Journal of Atmospheric and Solar-Terrestrial Physics*, 63:155–169.

Jessberger, E. K. e. a. (2001). *Interplanetary dust*, Chapter: Properties of Interplanetary Dust: Information from Collected Samples, pages 253–294. Astronomy and Astrophysics Library. Springer-Verlag, Heidelberg, Germany.

Jones, J., Brown, P., Ellis, K. J., Webster, A. R., Campbell-Brown, M., Krzemenski, Z., and Weryk, R. J. (2005). The Canadian Meteor Orbit Radar: System overview and preliminary results. *Planetary and Space Science*, 53:413–421.

Kero, J. (2008). *High-resolution meteor exploration with tristatic radar methods*. PhD thesis, Swedish Institute of Space Physics, Kiruna, Sweden.

Kero, J., Szasz, C., Pellinen-Wannberg, A., Wannberg, G., Westman, A., and Meisel, D. D. (2008a). Determination of meteoroid physical properties from tristatic radar observations. *Annales Geophysicae*. Submitted.

Kero, J., Szasz, C., Wannberg, G., Pellinen-Wannberg, A., and Westman, A. (2008b). On the meteoric head echo radar cross section angular dependence. *Geophysical Research Letters*. doi:10.1029/2008GL033402.

Meteor (1944). In *Ordbok över svenska språket utgiven av Svenska Akademien (SAOB)*, volume 17, pages 883–885. A.-B. PH. Lindstedts Univ.-bokhandel, Lund.

Mitchell, N. J. (2002). Meteor radar. In Holton, J. R., Curry, J. A., and Pyle, J. A., editors, *Encyclopedia of Atmospheric Sciences*, Chapter: Radar, pages 1819–1824. ACADEMIC PRESS.

Morton, J. D. and Jones, J. (1982). A method for imaging radio meteor radiant distributions. *Monthly Notices of the Royal Astronomical Society*, 198:737–746.

Murray, C. and Dermott, S. (1999). *Solar system dynamics*. Cambridge Univeristy Press, The Pitt Building, Trumpington Street, Cambridge, UK.

Öpik, E. J. (1958). *Physics of meteor flight in the atmosphere*. Number 6 in Interscience tracts on physics and astronomy. Interscience Publishers, Inc.

Pellinen-Wannberg, A. and Wannberg, G. (1994). Meteor observations with the European Incoherent Scatter UHF radar. *Journal of Geophysical Research*, 99(A6):11379–11390.

Rietmeijer, F. J. M. (2002). The earliest chemical dust evolution in the solar nebula. *Chemie der Erde*, 62:1–45.

Rogers, L. A., Hill, K. A., and Hawkes, R. L. (2005). Mass loss due to sputtering and thermal processes in meteoroid ablation. *Planetary and Space Science*, 53:1341–1354.

Roy, A. E. (1988). *Orbital motion*. Adam Hilger, Bristol and Philadelphia, 3rd edition.

Seidelmann, P., editor (1992). *Explanatory supplement to the astronomical almanac*. Univeristy Science Books, 20 Edgehill Rd; Mill Valley, CA 94941.

Singer, W., von Zahn, U., and Weiß, J. (2004). Diurnal and annual variations of meteor rates at the Arctic Circle. *Atmospheric Chemistry and Physics*, 4:1355–1363.

Tielens, A. G. G. M., McKee, C. F., Seab, C. G., and Hollenbach, D. J. (1994). The physics of grain-grain collisions and gas-grain sputtering in interstellar shocks. *The Astrophysical Journal*, 431:321–340.

Webster, A. R., Brown, P. G., Jones, J., Ellis, K. J., and Campbell-Brown, M. (2004). Canadian Meteor Orbit Radar (cmor). *Atmospheric Chemistry and Physics*, 4:679–684.

Westman, A., Wannberg, G., and Pellinen-Wannberg, A. (2004). Meteor head echo altitude distributions and the height cutoff effect studied with the EISCAT HPLA UHF and VHF radars. *Annales Geophysicae*, 22:1575–1584.

Wilkins, G. and Springett, A., editors (1961, Fourth impression (with amendents) 1977). *Explanatory supplement to the astronomical ephemeris and the American ephemeris and nautical almanac*. Her Majesty's Stationary Office, London. Issued by H.M. Nautical Almanac Office by Order of the Science Research Council.

Williams, I. P. (2002). *Meteors in the Earth's atmosphere*, Chapter: The evolution of meteoroid streams, pages 13–32. Cambridge University Press, Cambridge, UK.

Zeilik, M. and Gregory, S. A. (1998). *Introductory astronomy & astrophysics*. Saunders College Publishing, 4th edition.

Zhou, Q., Tepley, C. A., and Sulzer, M. P. (1995). Meteor observations by the Arecibo 430 MHz incoherent scatter radar - 1. Results from time-integrated observations. *Journal of Atmospheric and Terrestrial Physics*, 57:421–431.

A P P E N D I X

A Variable Name Key - Orbit Calculations

This is a translation key of variable names used in the meteoroid orbit calculations between Section 6 and the Matlab code KirunaAltAzr6.m. The variable names are in order of appearance.

$R_\oplus$ = aE	δ = delta2	n = n
$\omega_\oplus$ = wRT	c_X = cX	$\lambda_\odot$ = lambdas
Λ = Lambda	c_Z = cZ	d_{X_1} = dX
Φ = Phi	h = h	d_{Y_1} = dY
ϕ = phi, delta1	α = alpha2	d_{Z_1} = dZ
H = hh	Δ_α = Delta_alpha	γ = gamma
C = see	Δ_δ = Delta_delta	d_Q = dQ
ρ_{cv} = rho3	α_1 = alpha3	V_h = vee
r_{cv} = rp	δ_1 = delta3	N = nn
az = az	h_1 = hangle	d_{X_2} = cLX
zd = zd	c_{X_1} = zCX	d_{Y_2} = cLY
V_∞ = gvee1	c_{Y_1} = zCY	d_{Z_2} = cLZ
V_{east} = eastV	c_{Z_1} = zCZ	β_0 = beta0
ΔV = Delta_V	alt_1 = alt3	λ_0 = lambda0
V_g = gvee2, gvee	zd_1 = zD3	c_L = cI
$l_\odot$ = lS	V_2 = vg	s_L = sI
$m_\odot$ = mS	Ψ = Psi	I^2 = pL
$e_\odot, e_\oplus$ = ec	az_2 = az4	i = ii
$\omega_\odot$ = wS	zd_2 = zD4	c_ν = cV
JD = jD	alt_2 = alt4	s_ν = sV
t_0 = to	c_{X_2} = cX	a = aa
$E_\odot$ = eS	c_{Y_2} = cY	e = ecc
$r_\odot$ = rS	c_{Z_2} = cZ	Q = q
$v_{\odot x}$ = xp	h_2 = h3	q = qp
$v_{\odot y}$ = yp	δ_2 = delta	ν = nu
$v_\odot$ = v0	α_2 = alpha	E = eee
l_{apex} = lAP	c_{X_2} = cX	Δt = Delta_T, ttt
ε = epsilon	c_{Y_2} = cY	Ω = Omega0
alt = alt	c_{Z_2} = cZ	ω = w
θ_1 = Theta2	β = beta	T = period
c_Y = cY	λ = lambda	